This is a repository copy of *Observation of anomalous Meissner screening in Cu/Nb and Cu/Nb/Co thin films*.

White Rose Research Online URL for this paper:
http://eprints.whiterose.ac.uk/130938/

Version: Accepted Version

## Article:

# Observation of anomalous Meissner screening in Cu/Nb and Cu/Nb/Co thin films

M. G. Flokstra[1], R. Stewart[1], N. Satchell[2], G. Burnell[3], H. Luetkens[4],
T. Prokscha[4], A. Suter[4], E. Morenzoni[4], S. Langridge[2] and S. L. Lee[1]

[1]*School of Physics and Astronomy, SUPA, University of St.Andrews,
St.Andrews KY16 9SS, United Kingdom.* [2]*ISIS,
Rutherford Appleton Laboratory, Oxfordshire OX11 0QX,
United Kingdom.* [3]*School of Physics and Astronomy, University of Leeds,
Leeds LS2 9JT, United Kingdom.* [4]*Labor für Myonspinspektroskopie,
Paul Scherrer Institut, CH-5232 Villigen PSI, Switzerland.*
(Dated: May 15, 2018)

We have observed the spatial distribution of magnetic flux in Nb, Cu/Nb and Cu/Nb/Co thin films using muon-spin rotation. In an isolated 50 nm thick Nb film we find a weak flux expulsion (Meissner effect) which becomes significantly enhanced when adding an adjacent 40 nm layer of Cu. The added Cu layer exhibits a Meissner effect (due to induced superconducting pairs) and is at least as effective as the Nb to expel flux. These results are confirmed by theoretical calculations using the quasiclassical Green's function formalism. An unexpected further significant enhancement of the flux expulsion is observed when adding a thin (2.4 nm) ferromagnetic Co layer to the bottom side of the Nb. This observed cooperation between superconductivity and ferromagnetism, by an unknown mechanism, forms a key ingredient for developing superconducting spintronics.

The two defining characteristics of superconductivity are the absence of electrical resistance and the ability of the superconductor to expel magnetic fields (the Meissner effect). In mesoscopic superconducting systems the expulsion of magnetic fields can be very different from the bulk behavior. In normal-metal (N) superconducting (S) bilayers the N layer can exhibit a Meissner effect[1, 2] due to superconducting correlations entering the N layer through the proximity effect[3]. It was theoretically predicted that replacing the normal metal by a ferromagnet (F) can result in a paramagnetic (or inverse) Meissner effect[4] due to the presence of (time-reversed) spin-triplet correlations. Similar results had already been predicted for NS bilayers with a spin-active interface[5]. This paramagnetic Meissner effect, where flux is added rather than expelled, has been observed in a recent experiment[6] using low-energy muon-spin spectroscopy (LE-$\mu$SR), which is an exquisite tool to probe the local magnetic flux inside a thin film. In a related experiment on NSFnF (n = thin non-metallic spacer) structures, a magnetic flux lowering was observed inside the N layer with a dependence on the degree of non-collinearity between the F layers[7]. This could not be explained by an ordinary Meissner effect and is unanticipated by the quasiclassical theory framework for SF proximity systems. In a recent theory paper[8] the influence of spin-orbit coupling in an N layer on the (induced) Meissner effect was investigated and shown to exhibit anisotropic behavior.

In this letter we present LE-$\mu$SR measurements on S, NS and NSF thin films to disentangle the contributions to the magnetic flux expulsion from the various layers. For all structures S = Nb(50), N = Cu(40) and F = Co(2.4) with numbers indicating the layer thickness in nm. Two sets of samples were grown (labelled I and II) where for II a higher purity Nb target (99.999% instead of 99.99%) was used resulting in an increase in the Nb

mean-free-path of about 25% compared to I. We observe the counterintuitive result that the Nb single layer thin films expel the least field while the Cu/Nb/Co trilayer thin films expel the most. For the Nb single layers we find a small Meissner expulsion with a field penetration depth of 270 nm (I) and 160 nm (II) respectively. These value are much larger than the typical 30 nm found for clean Nb systems[9–11] but are not inconsistent with results on dirty systems (similar to those considered here) where the penetration length increases with decreasing mean free path and values up to 230 nm have been observed[12, 13]. For the Cu/Nb bilayers we find an enhancement of the Meissner expulsion, which we verify by theory. For the Cu/Nb/Co trilayers we surprisingly find a *further* enhancement of the magnetic flux expulsion, which is an order of magnitude larger compared to the Nb single layers. This enhancement is unanticipated by theory and shows a cooperation between the superconducting and ferromagnetic states, which is an essential ingredient for developing superconducting spintronics. This enhancement in our mesoscopic systems also forms a sharp contrast to observation on bulk Nb systems where a reduction of a (otherwise fully developed) Meissner state can occur as a result of flux trapping or inhomogeneous strayfields[14, 15].

Our samples were prepared by DC magnetron sputtering on Si (100) substrates in a system with a base pressure of $10^{-8}$ mbar at ambient temperature and in a single vacuum cycle. Growth of all layers was performed at a typical Ar flow of 24 sccm and pressure of 2-3 $\mu$bar with a typical growth rate of 0.2 nms$^{-1}$. Growth rates for each material were calibrated by fits to Kiessig fringes obtained by low angle X-ray reflectivity measurements on single material layers. Fig.1 shows resistance and critical field measurements for sample set II. From the critical field, the Ginzburg-Landau coherence length is determined and yields $\xi_{GL} = 11.1$ nm (for sample set

I we found $\xi_{GL} = 10$ nm).

The LE-$\mu$SR measurements were performed on the $\mu$E4 beamline at the Paul Scherrer Institut[16]. The muon is an unstable spin-$\frac{1}{2}$ lepton of charge $+e$ with a lifetime $t_\mu = 2.197$ $\mu$s and on decay it emits a positron preferentially along its momentary spin direction. Upon implantation into a material a muon will rapidly thermalize, while maintaining its spin direction, after which its spin precesses around the local field making it a local magnetic probe. By monitoring the decay positrons of implanted, 100% spin polarized muons, information about the precession frequency (and thus the local field) can be obtained. The implantation depth profile (or stopping profile) of the muon is energy dependent and can be calculated by a well-proven Monte-Carlo simulation[17, 18]. This allows the average probing depth to be tuned from about 10 to 100 nm below the surface. For a typical measurement several million counting events are collected at a rate of about 1k/s and errors as small as 0.1 G can be achieved[19] (see Suppl. Mat. for an example measurement and additonal information). All our muon measurements were undertaken in transverse field geometry (applied field orthogonal to the muon spin direction) with the applied field direction in the plane of the sample. From the measurement data taken at a particular muon energy $E$ (and thus a particular probing depth profile) one can determine the average flux $\langle B \rangle (E)$, which can also be presented as $\langle B \rangle \langle x \rangle$ with $\langle x \rangle$ the average probing depth of the muons at energy $E$. For our bi- and trilayers we use this (conventional) approach to treat the data. In cases where the shape of the flux profile is known, one can treat the measurement data imposing the analytical form of $B(x)$ to find the correct field profile rather then the weighted averages. This approach we use for the single Nb films at $T < T_c$, where the flux profile follows straightforwardly from the London equation and is given by

$$B(x) = B_0 \cosh\left(\frac{x}{\lambda} - \frac{d_S}{2\lambda}\right) \cosh\left(\frac{d_S}{2\lambda}\right)^{-1} \quad (1)$$

with $\lambda$ the field penetration depth, $d_S$ the Nb thickness and $x = 0$ corresponding to the top surface[3]. This thus allows the determination of the magnetic field penetration depth.

To compare our observed flux profiles with theory we use the quasiclassical framework in the dirty limit (coherence length much longer than mean free path) and apply the linear reponse theory to calculate the response to a small external field. In the dirty limit the Green functions obey the Usadel equation [20]. We take the x-axis normal to the metallic layers and assume translational invariance in the y,z plane. The Usadel equation for s-wave superconductivity then takes the form $i\hbar D\partial_x(\check{g}\partial_x\check{g}) = [\check{H}, \check{g}]$ with $\check{g}$ the $4 \times 4$ matrix Green function in the Nambu $\otimes$ spin-space, $\hbar$ the reduced Planck constant and $D$ the diffusion constant. When dealing with a homogeneous ferromagnetic exchange field, the Hamiltonian can be described by $\check{H} =$
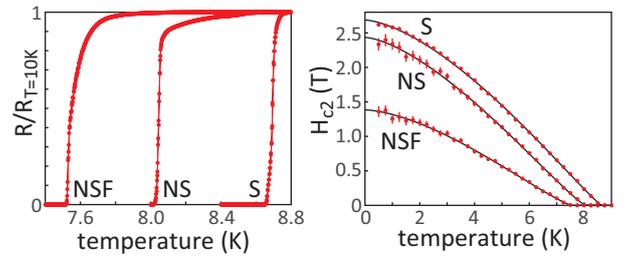


FIG. 1: Resistance (left) and critical field (right) measurements for sample set II (see text). Resistance is normalized to the resistance at $T = 10$ K and for the critical field the field direction was perpendicular to the sample plane.

$i\hbar\omega_n (\tau_3 \otimes \sigma_0) + \check{\Delta} - J_z\tau_0 \otimes \sigma_3$ (see e.g. [21]) with $J_z$ the exchange field directed along the z-axis and $\omega_n$ the Matsubara frequencies defined by $\hbar\omega_n = \pi k_B T (2n + 1)$ with $k_B$ the Boltzmann constant, $n$ integer and the maximum allowed frequency given by the Debye frequency. Furthermore, $\sigma_i$ and $\tau_i$ are the Pauli matrices of the spin space and Nambu space respectively. The matrix Green function and $\check{\Delta}$ only have non-zero elements on their main and anti-diagonals with diag($\check{G}$) = $(G_{\uparrow\uparrow}, G_{\downarrow\downarrow}, \overline{G}_{\uparrow\uparrow}, \overline{G}_{\downarrow\downarrow})$, anti-diag($\check{G}$) = $(F_{\uparrow\downarrow}, F_{\downarrow\uparrow}, \overline{F}_{\uparrow\downarrow}, \overline{F}_{\downarrow\uparrow})$ and anti-diag($\check{\Delta}$) = $(-\Delta, \Delta, -\Delta^*, \Delta^*)$, where $G$ and $F$ are the quasiclassical normal and anomalous Green functions respectively, both being functions of $(x, \omega_n)$, $\Delta(x)$ is the order parameter and up/down arrows indicate spin-up/spin-down. The matrix Green function satisfies the normalization condition $\check{g}^2 = \check{1}$ and the order parameter must be solved self-consistently satisfying the gap equation:

$$i\Delta(x) = \frac{\pi k_B T}{\ln\left(\frac{T}{T_{c0}}\right) + \sum_n\left(\frac{1}{|2n+1|}\right)} \sum_{\omega_n} F_{\uparrow\downarrow}(x, \omega_n) \quad (2)$$

with $T_{c0}$ the bulk critical temperature. We use the interface boundary conditions as formulated by Nazarov[22], which for the interface between two materials with labels $l, r$ for the layer on the left and right side of the interface respectively can be written as: $\sigma_l\check{g}_l\partial_x\check{g}_l = \sigma_r\check{g}_r\partial_x\check{g}_r$ and $\sigma_l\check{g}_l\partial_x\check{g}_l = \frac{2}{R_b}\frac{[\check{g}_l,\check{g}_r]}{4+\Gamma(\check{g}_l\check{g}_r+\check{g}_r\check{g}_l-2)}$, with $\sigma_i$ the conductivity of layer $i$, $0 \leq \Gamma \leq 1$ the interface transparency and $R_b$ the interface resistance times the interface area. When the Green functions are known one can calculate the response of the superconductor to a (small) external field. Within the linear reponse theory, the shielding current density $j_y(x)$ in response to the vector potential $A_y(x)$ is written as[23]:

$$j_y = -\frac{N_0 e^2 D}{\hbar} A_y \pi k_B T \sum_{\omega_n} \Re\left(F_{\uparrow\downarrow}\overline{F}_{\downarrow\uparrow} + F_{\downarrow\uparrow}\overline{F}_{\uparrow\downarrow}\right) \quad (3)$$

with $N_0$ the normal state density of states near the Fermi energy. The vector potential is defined by $\mathbf{B} = \nabla \times \mathbf{A}$ and using Maxwell's equation $\nabla \times \mathbf{B} = \mu_0\mathbf{j}$, the current density must thus satisfy $\mu_0\mathbf{j} = \nabla \times (\nabla \times \mathbf{A})$. Using both

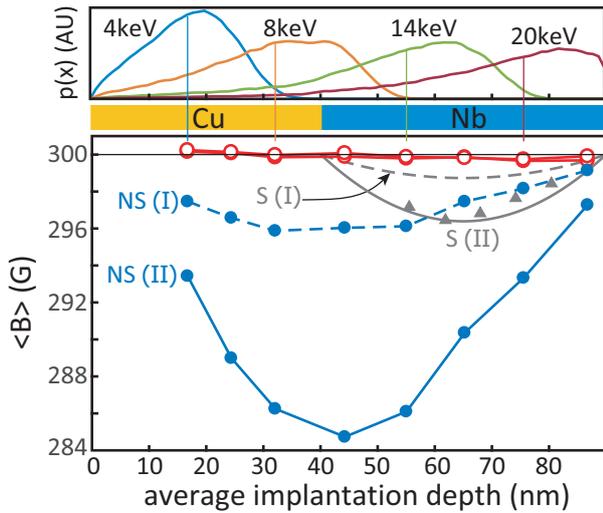expressions for the current density the vector potential (and thus the magnetic flux **B**) can be solved.



FIG. 2: Top panel: muon stopping profiles for the Cu/Nb bilayer for several implantation energies with their respective average implantation depth marked on the x-axis. For $E = 20$ keV and above, the profiles extend into the Si substrate (not shown). Bottom panel: results of the LE-$\mu$SR measurements presenting the obtained average flux $\langle B \rangle$ as function of the average implantation depth. Open(closed) round symbols correspond to measurements taken at $T = 10$ K (2.5 K) for the bilayer samples (see text). The corresponding flux profiles at $T = 2.5$ K for the Nb single layers are labelled S (I) and S (II) with triangles the measured averages for the latter.

Results of the LE-$\mu$SR measurement on the Nb single layer and the Cu/Nb bilayer thin films are presented in Fig.2. In the top panel the muon stopping profile for the bilayer is shown for several of the measurement energies. At a muon energy of 4 keV (the lowest measured energy), muons stop within the first 35 nm of the bilayer (i.e. all stop in the Cu), with the highest stopping probability near 20 nm. For increasing muon energies the muons penetrate deeper into the bilayer but always a (small) fraction will stop somewhere within the Cu. Each stopping profile corresponds to an average implantation depth $\langle x \rangle$ and we typically plot the obtained $\langle B \rangle (E)$ as $\langle B \rangle (\langle x \rangle)$. In the bottom panel these $\langle B \rangle (\langle x \rangle)$ for the bilayers are presented by open(closed) round symbols which corresponds to measurements taken at $T = 10$ K (2.5 K). At $T = 10$ K nothing unusal happens and we simply recover the externally applied field (which was set to about 300 G). When cooling to below $T_c$ we measure a lowering of the flux for all measured energies clearly showing that the Meissner screening is extending well into the normal metal. Errorbars for $\langle B \rangle$ are plotted for all measurements, but are typically too small (0.1-0.3 G) to be seen. We now compare these results with measurements on the Nb single layer thin films where instead of $\langle B \rangle (\langle x \rangle)$ we can determine the actual profile

using Eq.1 (for $T < T_c$). The results are presented by grey lines and the obtained magnetic penetration depths are 270 nm (I) and 160 nm (II) respectively. Both show a much smaller flux expulsion compared to their respective Cu/Nb bilayer counterparts.
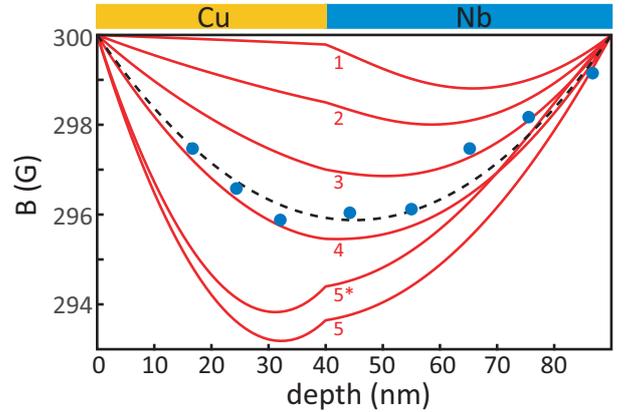


FIG. 3: Calculated flux profiles for a Cu(40)/Nb(50) bilayer for various values of the Cu mean free path $\ell$. All other material parameters were set to match those of the Cu/Nb bilayer of sample set I. Labels 1 to 5 correspond to $\ell = \{5, 11, 16, 22, 34\}$ nm. Curve 5* is calculated for a Cu(40)/Nb(50)/Co(2.4) trilayer with $\ell = 34$ nm and the dashed curve is calculated for a Nb(90) thin film. Round symbols are the NS (I) data from Fig.2

To compare our experimental results with theory we first calculate the Meissner flux expulsion for the Nb single layer (using the experimentally obtained values for $T_{c0}$ and $\xi_{GL}$) and finetune the Nb density of states such that the theory predicts the same flux expulsion as measured with the muons. For the Nb (I) we have $T_{c0} = 8.6$ K, $\xi_{GL} = \frac{\pi}{2} \sqrt{\frac{\hbar D}{2 \pi k_B T_{c0}}} = 10$ nm and find $N_0 = 4.0 \times 10^{28}$ m$^{-3}$. Next we repeat the process for the Cu/Nb bilayer. The parameters related to the interface boundary conditions are tuned to correctly predict the reduced $T_c$ of the bilayer. We used $\rho_{Nb} = 15.2$ $\mu\Omega$·cm, $\rho_{Cu} = 1.70$ $\mu\Omega$·cm, $\Gamma = 1$ and $R_b = 2.4 \times 10^{-15}$ $\Omega$·m$^2$. For the Cu density of states we find a value of $1.2 \times 10^{28}$ m$^{-3}$ and for the Cu mean-free-path $\ell$, which determines the Cu diffusion constant through $D = v_F \ell / 3$ with $v_F = 1.57 \times 10^6$ m·s$^{-1}$ the Fermi velocity for Cu[24], we find $\ell = 22$ nm. Finally we calculate the Meissner flux expulsion for the bilayer as function of $\ell$. Results of these calculations are presented in Fig.3. They clearly show that the normal metal exhibits a Meissner effect and that the amount of flux expulsion depends strongly on the material parameters. For curve 1 where the diffusion of Cooper pairs into the normal metal is strongly suppressed, the flux profile is nearly identical to S (I) from Fig.3. For increasing $\ell$, which allows Cooper pairs to diffuse further into the Cu, the ability of the Cu layer to expel flux increases and eventually the bilayer is more efficient compared to a single Nb layer with a thickness equal to that of the bilayer

(dashed curve in figure). The experimental $\langle B \rangle$ data of NS (I) from Fig.2 is represented by round symbols.
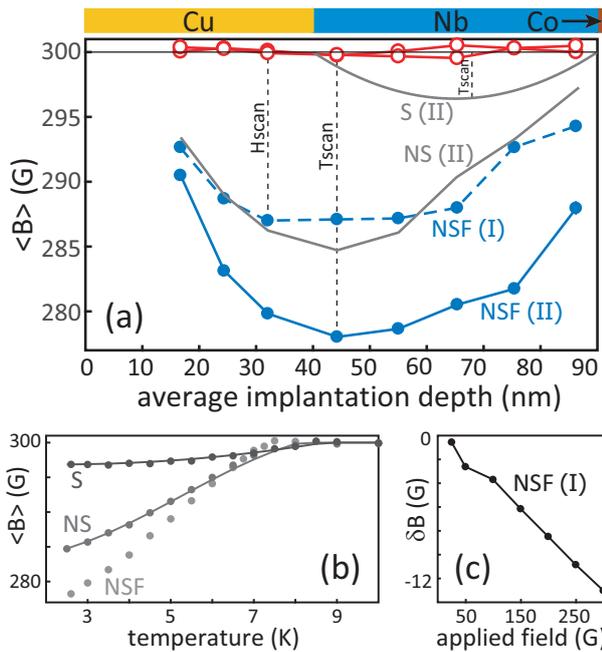


FIG. 4: (a) trilayer data presented in a similar fashion as in Fig.2 with the other results of sample set II from Fig.2 added for direct comparison. Tscan and Hscan mark the energies used to aquire the data presented in b and c. (b) $\langle B \rangle$ as function of temperature for all samples of set II. For the S and NS layout the predicted behaviour using the quasiclassical was calculated (solid lines) and makes an excellent fit to the data. (c) $\delta B = \langle B \rangle\,(T = 2.5\text{ K}) - \langle B \rangle\,(T = 10\text{ K})$ as function of applied field for the trilayer of sample set I.

We now add a ferromagnetic Co layer to the bottom side of the bilayer to form the Cu/Nb/Co trilayer. Given that the Co is a strong pair breaker, one might expect the flux expulsion to be reduced. Also, when considering the time-reversed character of the spin-triplet pairs which arise in this system it would again predict a reduction of the expulsion. Curve 5* in Fig.3 shows the theoretically obtained flux profile for such trilayer where the material parameters for the Cu and Nb are identical to those used for curve 5 and for Co we used $\xi_F = \sqrt{\hbar D_F / J_z} = 1$ nm, $J_z = 312$ meV. The Nb/Co interface parameters were tuned to match the experimentally obtained reduced $T_c = 7.6$ K of the trilayer. While theory indeed shows a reduction of the flux expulsion, experimentally we find quite the opposite. These results are presented in Fig.4a in a similar fashion as for Fig.2. Remarkably it shows a significant *increase* in the flux expulsion with a spatial profile that otherwise looks very similar to that found in the bilayer samples. To investigate further this unexpected flux expulsion we make measurements as a function of temperature and of applied field. The muon energies used for these measurements are marked in the figure by Tscan and Hscan respectively. The result of

the temperature dependence of $\langle B \rangle$, taken for all samples of set II, is shown in Fig.4b. It clearly shows that as function of temperature the external field isn't expelled until the temperature drops below $T_c$ (see Suppl. Mat. for a more detailed graph). For the S and NS case we calculate the temperature dependence of the flux expulsion (using material parameters obtained in a similar fashion as for sample set I) and find an excellent agreement between the quasiclassical prediction and the muon experiment (solid lines). For the NSF we note that below $T_c$, the amount of flux expulsion progresses in a linear fashion down to the lowest temperature we could reach. In Fig.4c we plot the size of the effect defined as $\delta B = \langle B \rangle\,(T = 2.5\text{ K}) - \langle B \rangle\,(T = 10\text{ K})$ as function of applied field for the trilayer of set I. It shows a very linear dependence down to an applied field of 20 G (the lowest field at which we measured) and extrapolates approximately to $\delta B = 0$ at zero applied field.

While the experimental results on the Nb and Cu/Nb thin films may be somewhat surprising, i.e. the flux expulsion of a mesoscopic superconductor can be *enhanced* by adding a normal metal to it, it is actually confirmed by theory. The result on the Cu/Nb/Co thin film however is unanticipated by theory and shows that the current understanding and description of SF proximity systems is missing a vital element. The trilayer shows a flux expulsion that grows linearly with applied field, which is similar to what is expected of a Meissner effect. However, the temperature dependence of the flux expulsion is also linear and it is not immediately obvious why that should be since the pair density does not develop linearly with temperature. Another noteworthy point is that while the LE-$\mu$SR measurements are sensitive to local flux, it does not discriminate between the origin being a screening current or, for example, aligned spins. This leaves open, for example, the possibility of a spin-current being driven by Meissner screening to explain the anomalous effect in the Cu/Nb/Co trilayer.

In conclusion, we have observed the spatial distribution of magnetic flux in Nb, Cu/Nb and Cu/Nb/Co thin films using LE-$\mu$SR. In the Nb(50) thin films we find a weak Meissner effect and only about 0.3-1% (depending on the quality of the Nb) of the applied field is expelled from the interior of the film corresponding to a field penetration depth of about 160-270 nm. For the Cu(40)/Nb(50) bilayer thin films we find the normal metal exhibiting a Meissner effect as well as a significant global *enhancement* of the flux expulsion from the interior. These results are confirmed by theoretical calculations. For the Cu(40)/Nb(50)/Co(2.4) trilayer thin films we find an unexpected (and unanticipated by theory) further enhancement of the expulsion, about an order of magnitude larger compared to the Nb(50) thin films. This observed cooperation between superconductivity and ferromagnetism, by an unknown mechanism, forms a key ingredient for developing superconducting spintronics.

[1] Y. Oda and H. Nagano, *Solid State Commun.* **35**, 631 (1980).

[2] W. Belzig, C. Bruder and G. Schön, *Phys. Rev. B* **53**, 5727 (1996).

[3] A. C. Rose-Innes and E. H. Rhoderick, *Introduction to Superconductivity* (Pergamon Press, 1994).

[4] M. Alidoust, K. Halterman and J. Linder, *Phys. Rev. B* **89**, 054508 (2014).

[5] T. Yokoyama, Y. Tanaka and N. Nagaosa, *Phys. Rev. Lett.* **106**, 246601 (2011).

[6] A. Di Bernardo, Z. Salman, X. L. Wang, M. Amado, M. Egilmez, M. G. Flokstra, A. Suter, S. L. Lee, J. H. Zhao, T. Prokscha, E. Morenzoni, M. G. Blamire, J. Linder and J. W. A. Robinson *Phys. Rev. X* **5**, 041021 (2015).

[7] M. G. Flokstra, N. Satchell, J. Kim, G. Burnell, P. J. Curran, S. J. Bending, J. F. K. Cooper, C. J. Kinane, S. Langridge, A. Isidori, N. Pugash, M. Eschrig, H. Luetkens, A. Suter, T. Prokscha and S. L. Lee, *Nat. Phys.* **12**, 57 (2016).

[8] C. Espedal, T. Yokoyama and J. Linder, *Phys. Rev. Lett.* **116**, 127002 (2016).

[9] G. P. Felcher, R. T. Kampwirth, K. E. Gray and R. Felici, *Phys. Rev. Lett.* **52**, 1539 (1984).

[10] A. Suter, E. Morenzoni, N. Garifianov, R. Khasanov, E. Kirk, H. Luetkens, T. Prokscha and M. Horisberger, Phys. Rev. B **72**, 024506 (2005).

[11] A. Romanenko, A. Grassellino, F. Barkov, A. Suter, Z. Salman and T. Prokscha, *Appl. Phys. Lett.* **104**, 072601 (2014).

[12] H. Zhang, J. W. Lynn, C. F. Majkrzak, S. K. Satija, J. H. Kang and X. D. Wu, *Phys. Rev. B* **52**, 10395 (1995).

[13] A. I. Gubin, K. S. Ilin, S. A. Vitusevich, M. Siegel and N. Klein, *Phys. Rev. B* **72**, 064503 (2005).

[14] H. Stalzer, A.Cosceev, C. Sürgers, H. v. Löhneysen, J.-M. Brosi, G.-A. Chakam and W. Freude, *Appl. Phys. Lett.* **84**, 1522 (2004).

[15] S. Aull, O. Ebrahimi, N. Karakas, J. Knobloch, O. Kugeler and W. Treimer, *Journal of Physics: Conference Series* **340**, 012001 (2012).

[16] T. Prokscha, E. Morenzoni, K. Deiters, F. Foroughi, D. George, R. Kobler, A. Suter and V. Vrankovic, *Nucl. Instr. and Meth. A* **595**, 317-331 (2008).

[17] W. Eckstein, Computer Simulation of Ion-Solid Interactions, Springer, Berlin, Heidelberg, New York, 1991.

[18] E. Morenzoni, H. Glückler, T. Prokscha, R. Khasanov, H. Luetkens, M. Birke, E. M. Forgan, Ch. Niedermayer and M. Pleines, *Nucl. Instr. and Meth. B* **192**, 254-266 (2002).

[19] P. Bakule and E. Morenzoni, *Contemporary Physics* **45**, 203 (2004).

[20] K. D. Usadel, *Phys. Rev. Lett.* **25**, 507 (1970).

[21] T. Löfwander, T. Champel, J. Durst and M. Eschrig, *Phys. Rev. Lett.* **95**, 187003 (2005).

[22] Y. V. Nazarov, *Superlattices Microstruct.* **25**, 1221 (1999).

[23] O. Narikiyo and H. Fukuyama, *J. Phys. Soc. Jpn.* **58**, 4557 (1989).

[24] C. Kittel, *Introduction to Solid State Physics, 7th Ed.* (Wiley, 1996).